Remote Sounding of High Clouds: II. Emissivity of Cirrostratus

C. M. R. PLATT AND A. C. DILLEY

CSIRO Division of Atmospheric Physics, Aspendale, Victoria, Australia

(Manuscript received 6 December 1978, in final form 29 April 1979)

ABSTRACT

The results from a series of measurements of the beam emissivity of cirrostratus at 10–12 μm wavelengths are presented, using methods of analysis which were discussed in Part I. A ruby lidar and infrared radiometer were used to gather data remotely from the ground. The various sources and magnitudes of error are discussed. The results for eight large cirrostratus systems which were observed on different days gave a mean beam emissivity of 0.54 (or flux emissivity of 0.70). This compares with a value of 0.245 (0.38 for flux obtained during an earlier period (Platt, 1973). The measurements were obtained at 35°S (Adelaide) and 38°S (Aspendale). The cloud systems at Aspendale all formed in similar synoptic situations.

1. Introduction

In a previous paper (Platt, 1979, hereafter referred to as Part 1), methods for calculating the optical properties of high ice clouds from remote ground-based measurements by lidar and radiometry were described. It was shown that the visible and infrared (IR) optical thicknesses at the lidar and radiometer wavelengths, respectively, the IR emissivity and the lidar backscatter profile could all be obtained.

In this paper we report the IR emissivity of cirrostratus systems, calculated from lidar and radiometer data on the basis of the methods of Part 1. Previous measurements on cirrus or cirrostratus (Kuhn and Weickmann, 1969; Davis, 1970; Allen, 1971; Platt, 1973, 1975; Cox, 1976) have revealed a wide range of values of IR emissivity. Cells embedded in the cloud shield with emissivities approaching unity have been observed by Platt (1973). Griffith and Cox (1977) recently have reported emissivities approaching unity in 1 km deep tropical cirrostratus.

The measurements reported here form part of a continuing program of observations and are intended as an interim data set for use with climate models. To the authors' knowledge, they are the first measurements on large midlatitude cirrostratus cloud systems as opposed to isolated cirrus clouds.

2. Experimental method

Some early measurements were made in 1972 at Adelaide (35°S) with the equipment described in Platt (1973). Later measurements were made with a new lidar installed at Aspendale (38°S) in 1975 (Allen and Platt, 1977). This system is controlled by a Hewlett-Packard 2100A computer. The lidar data are digitized by a BIOMATION 8100 transient recorder and stored on tape. All subsequent calculations are made on the CSIRO computer network.

The infrared radiometer design has not changed radically since the early measurements (Platt, 1971), although the more stable UNICAM IR50 Golay detector is now in use. The infrared (IR) data are digitized by the HP 2100A computer, together with the calibration blackbody temperature and the energy of each laser pulse.

During observation periods lidar profiles in the vertical were taken at 30 S or 1 min intervals as the clouds drifted overhead. The infrared radiometer measured the cloud radiance continuously, the data being recorded every second, except for a calibration period of 2 min every 20 min when a grooved calibration blackbody which was maintained at ambient temperature was moved automatically in front of the radiometer aperture. Measurements were not continued for the complete duration of any cloud system, but several hours of observation was typical. A requirement of the cloud system was that no other type of cloud be present.

At Aspendale the lidar and radiometer were placed 1 m apart and aligned accurately in the vertical to observe the same volume of the cloud. The lidar receiver and radiometer fields of view were 10 and 6 mrad, respectively. The lidar pulse energy was typically 1 J with about 20% rms variation. The vertical range resolution was set by an electronic filter following the photomultiplier detector and amplifier. The filter bandwidth was normally set at 5 MHz, giving a vertical resolution of 30 m. Aerological data was obtained from twice-daily ascents at stations within 50 km of the lidar.

0021-8952/79/091144-07$05.75

3. Analysis and errors

a. *Infrared data*

Methods of reducing the measured radiometric output voltage to a sky radiance have been described previously (Platt, 1971, 1973). The alternating radiation signal at the radiometer detector is proportional to the difference between the signal radiance and the radiance from a temperature-controlled reference blackbody which comprises half the aperture and which is maintained at 40°C.

The vertical downward radiance I_s at the ground can be written

$$I_s = \tau(I_c + I_g) + I_{\text{sky}}, \quad (1)$$

where τ is the transmittance between the cloud and ground, I_c the vertical radiance at cloud base due to cloud emission, I_g upwelling radiance from the ground which is reflected downward by the cloud, and I_{sky} the radiance of the clear atmosphere (due mainly to emission by water vapor) between the cloud and ground. In this equation, the sky radiance above the clouds is considered to be negligible because of both the low water vapor contents and low temperatures above cirrus clouds. All terms are spectral values in the 10–12 μm wavelength interval.

Since the value of I_{sky} is typically of the same order of magnitude as the term τI_c, its accurate determination is important. It is normally calculated from the radiometer output voltage when there is no cloud in the radiometer field of view (as checked by a lidar sounding). Most cirrus systems are sufficiently broken to give this condition at some time. If no clear patches occur, I_{sky} may be obtained by plotting the integrated lidar backscatter $\gamma'(\pi)$ (see Part I) against the measured radiance I_s and extrapolating I_s to zero to give $\gamma'(\pi)$.

A value of τ is determined by computing the sky radiance with a standard transfer equation together with local aerological data and a trial water vapor absorption coefficient and then adjusting this coefficient in the computation (allowing for e-type absorption) until the calculated sky radiance is consistent with the measured value. τ is then calculated from the final absorption coefficient and the water vapor content. τ varies typically between 0.7 and 0.9, depending on the atmospheric water vapor content.

The term I_g is estimated, as in Platt (1973), by computing the component of upwelling radiation from the earth's surface which is scattered vertically downward. Using the angular scattering phase function for cirrus due to Hall (1968), the vertical downward radiance backscattered from a number of upward directions between 180° and 90° scattering angle is computed and summed, to give the total radiance. Water vapor emission and absorption in the intervening atmosphere is also taken into account, using typical midlatitude profiles of temperature and humidity. Only single scattering is considered.

The value of I_g is computed for various values of $\delta_A(h)$, the cloud IR optical depth. The earth's surface is assumed to be a blackbody at temperature T and the effective radiance, as observed through the 10–12 μm filter of the radiometer, is calculated.

I_g can be represented to within 1% by

$$I_g = D(T)[1 - e^{-2.3\delta_A(h)}],$$

where $D(T)$ is a function of surface temperature T and is equal to the effective reflected radiance in the downward beam when the cloud becomes "black." For the 10–12 μm filter used in the radiometer and for surface temperatures from about 5–30°C, $D(T)$ is given by

$$D(T) = 5.07\times10^{-3} + 9.16\times10^{-5}T + 5.06\times10^{-7}T^2.$$

For $T = 20$°C, $I_g = 0.0071$ mW cm^{-2} sr^{-1}. For a cloud emissivity of 0.5, I_g represents 11% of I_c for a cloud at -50°C and 7% for a cloud at -30°C.

b. *Lidar data*

The method and theory of the calibration of the lidar system has been given in Part 1. The lidar returns are calibrated in terms of the clear atmosphere at an altitude ($\sim$10 km) where the aerosol content is a minimum. The contributions from molecular backscatter and the background sky radiance are subtracted from the lidar profiles. The measured cloud backscatter coefficients $B'(\pi,z)$ are then integrated through each cloud profile to give the measured integrated backscatter $\gamma'(\pi)$. The cloud boundaries, which appear as sudden departures of the backscatter signal from the molecular level, are determined manually.

c. *Infrared emissivity (10–12 μm)*

The infrared emissivity was calculated by the method described in Part 1.

The basis of the method is the calculation of the downward IR radiance at cloud base using the corrected lidar backscatter profile to give the variation of the infrared absorption coefficient with altitude. It is assumed that the ratio g of the IR absorption coefficient to the lidar backscatter coefficient is the same at all altitudes. The calculated radiance is then tuned to the measured radiance by the variation of g in the computation. The IR emissivity is then calculated from the calculated IR absorption optical depth. A small correction is made for the effects of cloud particle scattering of the radiation.

The lidar backscatter profile is corrected for pulse attenuation by using an experimentally measured backscatter to extinction ratio k_a. This ratio is obtained from a plot (such as shown in Fig. 2a or 2b) of the integrated backscatter $\gamma'(\pi)$ against the IR emissivity ϵ. This means initially one requires an *a priori* value of k_a, which can be obtained from previous results (e.g., Platt, 1973). Having obtained a plot of $\gamma'(\pi)$ vs ϵ for

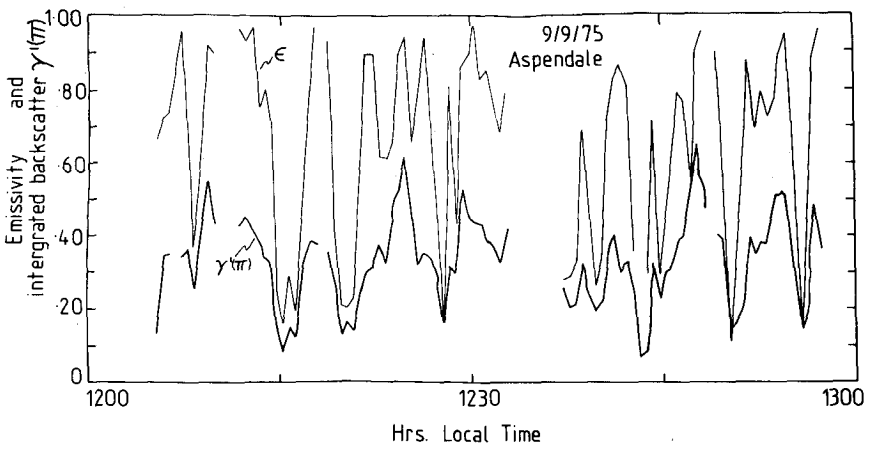

FIG. 1. Time variations in the values of vertical IR emissivity ϵ and vertical lidar backscatter $\gamma'(\pi)$ during one run, showing the large and frequent changes in these values which were often observed.

one system using the above value of k_a, a better value of k_a can be obtained as twice the average value of $\gamma'(\pi)$ when ϵ tends to unity. The calculation of ϵ is then repeated to give a more accurate value.

Fig. 1 shows variations in the integrated lidar backscatter $\gamma'(\pi)$ with time and the corresponding variations in the calculated (final) emissivity ϵ. Plots of $\gamma'(\pi)$ vs ϵ for individual times for two separate occasions are shown in Figs. 2a and 2b.

The total predicted errors in ϵ and their dependence on the value of ϵ are shown in Fig. 3, for three different cloud temperatures. The total experimental errors include radiometer noise fluctuations, pointing errors, radiometer calibration errors, errors in the atmospheric transmittance below the cloud, etc. Systematic calibration errors in the lidar backscatter coefficient hardly affect the accuracy of the emissivity calculation. For low values of ϵ, errors in the measurement of radiance predominate; errors from inaccuracies in the calculation of lidar backscatter coefficients (due to uncertainties in k_a) only become significant above $\epsilon \approx 0.4$.

The predicted errors are shown as error bars in Figs. 2a and 2b. They account for a large part of the observed scatter. It is probable that excess scatter in the data points is due to variations in the value of the backscatter-to-extinction ratio in the cloud.

4. Results

Results from the two observation periods are shown in Table 1 in the form of the frequency of the measured

TABLE 1. Frequency of measured emissivity within the intervals shown.

	Adelaide (1972)			Aspendale (1975)					
Emissivity interval	6 May	7 May	13 May	1 Sep	8 Sep	9 Sep	28 Oct	13 Nov	Total
0–0.1	29	0	44	0	0	20	0	5	98
0.1–0.2	29	0	3	9	0	20	2	9	72
0.2–0.3	34	11	16	16	0	13	10	6	106
0.3–0.4	32	10	16	32	0	24	13	8	135
0.4–0.5	28	15	5	48	8	18	2	8	132
0.5–0.6	26	23	1	51	21	17	7	9	155
0.6–0.7	14	14	0	27	44	32	8	7	146
0.7–0.8	5	10	0	27	15	35	9	2	103
0.8–0.9	2	22	0	9	8	37	22	0	100
0.9–1.0	10	43	0	8	2	28	40	0	131
									1178
Mean cloud base (km)	9.2	9.2		4.7	6.6	6.5	8.6	6.4	
Mean cloud thickness (km)	3.7	3.3		2.2	3.4	2.2	2.3	1.7	
Mean temperature (°C)	−50	−52		−26	−37	−34	−46	−26	
Mean emissivity	0.38	0.83	0.18	0.53	0.51	0.56	0.71	0.47	
Overall mean emissivity									0.49

emissivity within intervals of 0.1. The average cloud base, depth and temperature are also shown. Mean properties for some of the systems are shown schematically in Figs. 4a–4c.

During the observation periods, every suitable cloud system was sampled, mainly during daylight hours.

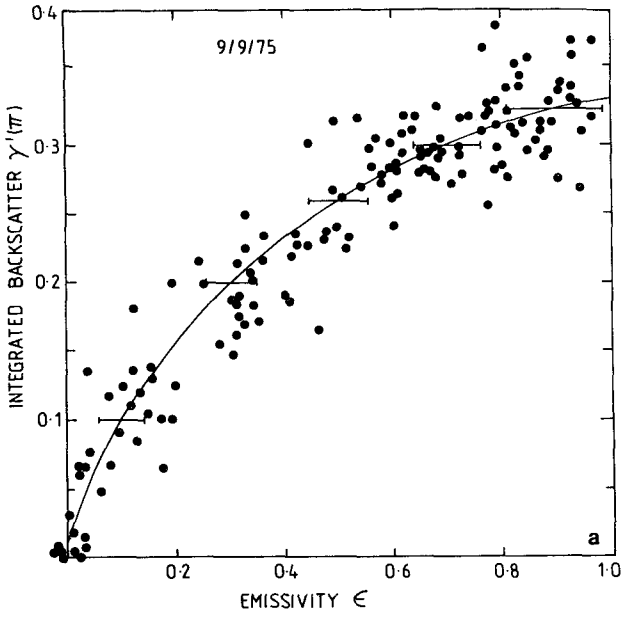

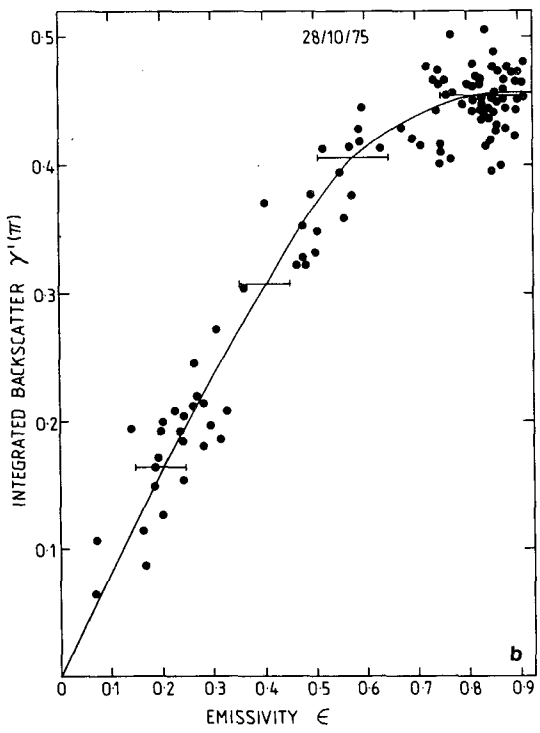

FIG. 2. Plots of $\gamma'(\pi)$ versus corresponding values of ϵ for 9 September 1975(a) and 28 October 1975(b). The error bars are predicted values (see text).

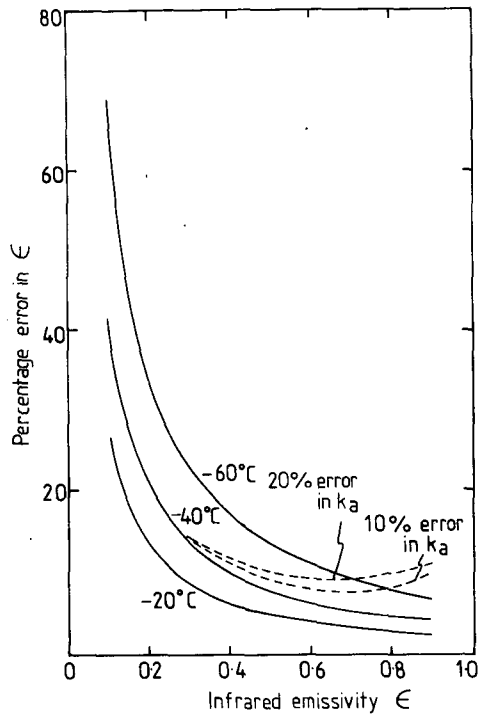

FIG. 3. Curves of predicted errors in ϵ for clouds at three different temperatures plotted against ϵ. Solid line: radiometric errors; dashed line: errors involved in the calculation of ϵ from the lidar data (at −40°C).

On one day in October 1975 the lidar malfunctioned and the results were not included.

The lidar and radiometer data were very carefully examined before being included in the analysis.

The cirrostratus observed at Adelaide on 6–7 May 1972 was very extensive, covering much of southern East Australia. The cloud was very deep, and its mean temperature quite low. An interesting feature was that although the cloud height and depth remained rather similar, the cloud had a much higher average emissivity on the 7th than it did on the 6th. This change could have reflected the evolution of the cloud with time, assuming that the system could be treated as one entity. On the other hand, it might have indicated the movement of the entire system, so that a more active part of the cloud was over Adelaide on the 7th.

On 13 May the cirrostratus was observed ahead of an approaching front and the cloud thickness and emissivity gradually increased with time.

The clouds observed at Aspendale in spring 1975 were all large cirrostratus systems which covered the entire sky for periods varying from several hours to a whole day. For these systems, the average emissivity was rather similar, although the cloud height, thickness and temperature varied considerably. The cloud of 1 September was quite low, and would probably be classified as "false cirrus," as it had the typical appearance of cirrus, but its altitude classified it more as a

mid-level cloud. In some systems, such as on 9 September, the cloud consisted of large horizontal billows aligned roughly normally to the direction of the wind.

The present results are compared in Fig. 5 with those reported in Platt (1973) from a previous study at Adelaide in November 1970. Both the distribution and the mean emissivity are different for the two histograms. In 1970, three of the four systems would have been classified as closer to cirrus than cirrostratus, which may explain some of the difference. Also, the 1970 systems were measured in early summer rather than autumn or spring. The mean weighted beam emissivity for the two sets of data is 0.40.

A glance at the mean values of temperature, emissivity and cloud thickness in Table 1 would seem to indicate little correlation between these quantities. This is in agreement with earlier findings. A fuller investigation of this aspect is at present in progress with the use of a new and larger data set.

5. Discussion and conclusions

The results presented here indicate the great variability of cirrus emissivity both spatially and temporally. Some systems contained large areas where the emissivity did not exceed 0.1, whereas in other systems, large areas occurred where the emissivity approached unity. This variability must obviously be associated with the moisture supply, vertical velocity and other mesoscale features associated with the synoptic situation. In this context, we consider the 6–7 May episode in more detail. The change in mean emissivity between 6 and 7 May represented a change in mean absorption coefficient from 0.13 ($\epsilon=0.38$) to 0.54 km^{-1} ($\epsilon=0.83$),

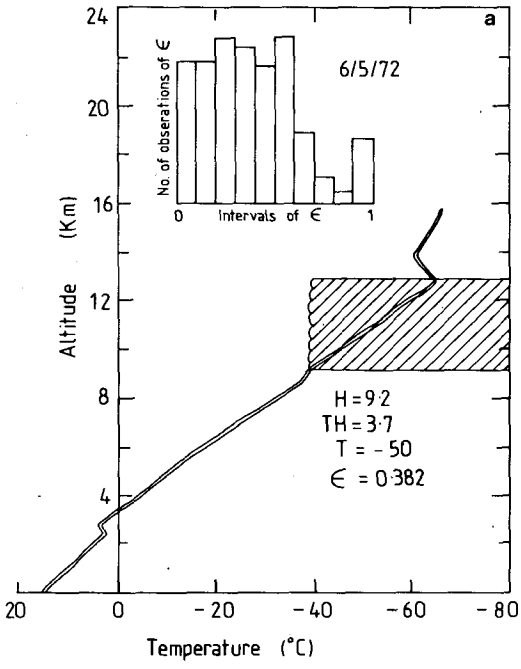

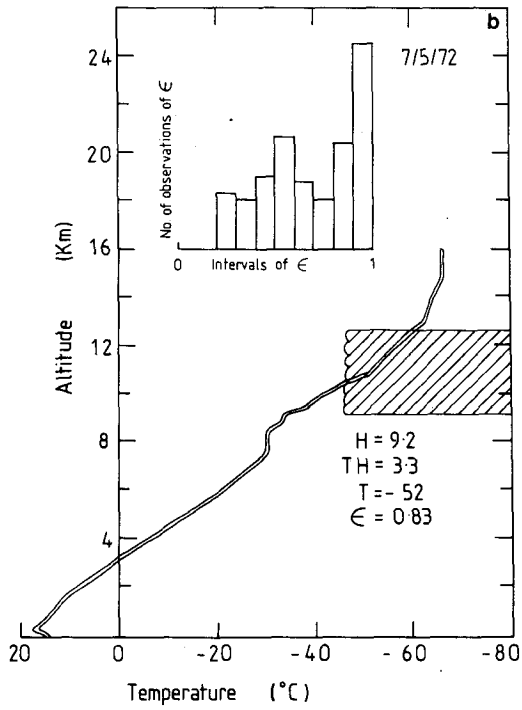

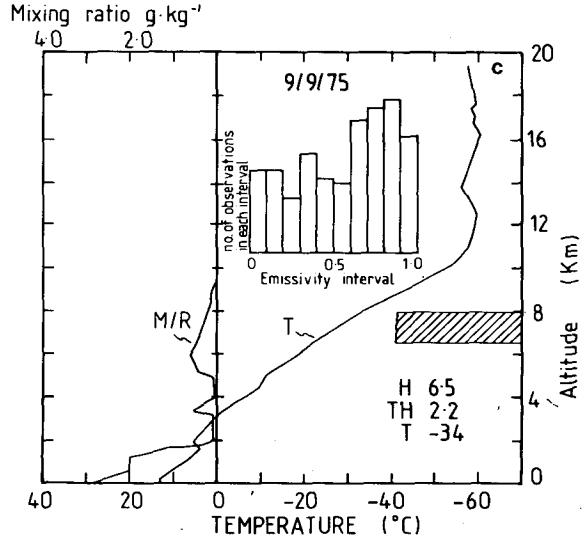

FIG. 4. Mean values of cloud thickness TH, base height H, temperature T, and emissivity ϵ together with emissivity histograms and aerological data for 6 May 1972(a), 7 May 1972(b) and 9 September 1975(c).

which is approximately a factor of 4. In terms of the cloud microphysics, the change is due either to an increase in particle number density n or in particle size r or a combination of both. However, any changes in absorption coefficient are also constrained by the available water content W of the cloud. Consider, for simplicity, a monodisperse cloud of particles of radius r. Suppose first that n changes but W remains constant; then the particle radius must decrease according to the relation

$r=(3W/4\pi n)^{\frac{1}{3}}$. For particles large compared to the wavelength, the absorption coefficient $\sigma_A=\pi r^2 n=\pi(3W/4\pi n)^{\frac{2}{3}}\, n$ and therefore $\sigma_A \propto n^{\frac{1}{3}}$. Thus, although σ_A does increase, n must change by a factor of 64 in order that σ_A increase by a factor of 4. Such changes in concentrations have not been observed in natural cirrus clouds (Heymsfield and Knollenberg, 1972).

Consider now that W (i.e., r) increases, but n remains constant. For σ_A to increase by a factor of 4, r must increase by a factor of 2, and W must therefore increase by a factor of 8. Such an increase in W could occur if the lifting processes in the cloud became more vigorous. For the cloud in question, lifting of air adiabatically from the cloud base at ~ -40°C to the cloud top at ~ -60°C would cause about 0.11 g m^{-3} of liquid (ice) to condense. Assuming that a cirrus particle has an equivalent radius of 50 μm (Platt, 1973), then for $W=0.11$ g m^{-3}, $\sigma_A=1.65$ km^{-1}. Thus, the values of σ_A observed were well below the adiabatic limit, and the measured differences in σ_A could certainly be accounted for in terms of the dynamic vigour of the cloud.

The particle measurements of Heymsfield and Knollenberg (1972) in four cirrus systems gave a factor of 4 between the lowest and highest value of W and a factor of 2 in the mean concentration. Thus, increases in σ_A appear to be due to a combination of an increase in number concentration and liquid water content. It is interesting that the mean sizes of the crystals measured by the above authors did not vary much indicating that the crystal size may be determined by factors other than the available adiabatic ice content.

It appears that most cirrostratus systems form ahead of surface fronts; thus the associated mechanism obviously is important to the understanding of cirrostratus formation at this latitude. It is not clear at present as to whether the mechanism is directly associated with a jet stream. It also appears that cirrostratus is much more prevalent than isolated cirrus at this latitude, although more observations are needed to establish the relative importance of the two types. In this context, there is often considerable doubt as to which category to use for a given situation,

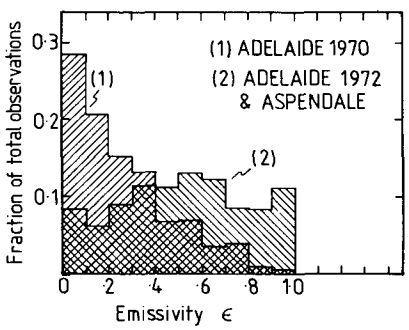

FIG. 5. Histograms of emissivity, comparing the distribution from the study at Adelaide (Platt, 1973) and that from the present data.

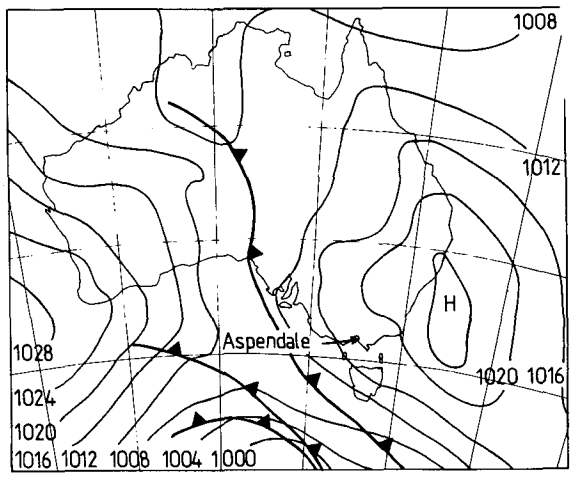

FIG. 6. A surface analysis of the Australian region on 28 October 1975 when a large cirrus system was passing over Aspendale.

particularly just ahead of a large system, when the cirrus/cirrostratus first appears. A typical synoptic situation when cirrus clouds were situated over Aspendale is shown in Fig. 6.

The quantity measured in this study was the beam emissivity, whereas a more useful quantity for climatic and dynamic modeling of clouds is the flux emissivity ϵ_F. An approximation for ϵ_F which assumes a horizontally homogeneous cloud and which neglects scattering is

$$\epsilon_F=\frac{\int_0^1 \{1-\exp[-\delta_A(h)\sec\theta]\}\cos\theta d(\cos\theta)}{\int_0^1 \cos\theta d(\cos\theta)}. \quad (2)$$

This equation simply integrates the radiance over zenith angle. Reasonable agreement has been obtained between values of ϵ_F using Eq. (2) and values using a more rigorous multiple-scattering calculation (see Paltridge and Platt, 1976). The relationship between ϵ_F and ϵ is shown in Fig. 7. The ϵ_F corresponding to $\epsilon=0.40$ is $\epsilon_F=0.57$.

Radiation divergence and the associated heating/cooling at the cloud boundaries can have a large effect on a cloud's equilibrium situation and its subsequent evolution (e.g., Paltridge and Platt, 1976). Particularly interesting in this context is again the 6–7 May episode at Adelaide in 1972. Referring to Figs. 4a and 4b, the clouds over Adelaide became progressively more emissive from the 6th to the 7th. The temperature profile on the 7th shows considerable modification compared to the 6th, with a large depth of heating near the cloud base. Although this heating could have occurred through advection, theoretical calculations show that cloud radiative interchange with surface radiation can also explain the observed heating.

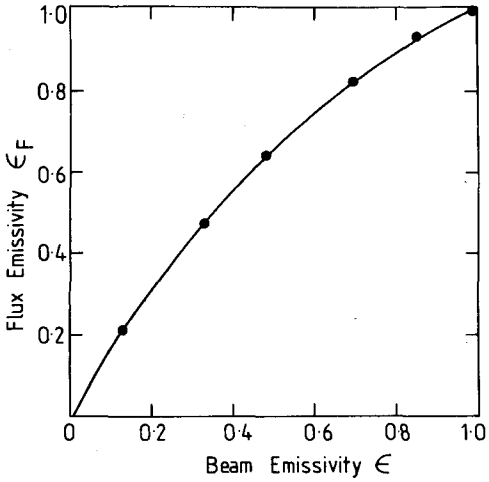

FIG. 7. The relation between flux emissivity ϵ_F and beam emissivity as given by Eq. (3) (see text).

It is thus at least possible that a significant fraction of total radiant energy gain is going into sensible heat, causing a stable layer to form at the cloud base. This effect is not so evident in Fig. 4c, although a small inversion is apparent near cloud base.

The prevalence of regions of high emissivity in many of the systems confirms the findings of previous investigators (Platt, 1973; Hubert, 1975; Griffith and Cox, 1977). However, the fact that the emissivity does not approach unity in every system means that satellite interpretation of cirrus IR brightness temperatures must always be treated with care.

The overall mean flux emissivity of 0.57 is quite high and indicates that the cirrostratus systems observed are important modulators of the earth's radiative energy budget.

Acknowledgments. The assistance of Mr. Stewart Young, Dr. Karel Bartusek and Mr. Leon Thomas, all of whom obtained the lidar results at Adelaide, is gratefully acknowledged.

REFERENCES

Allen, J. R., 1971: Measurements of cloud emissivity in the 8–13 μm waveband. *J. Appl. Meteor.*, **10**, 200–265.

Allen, R. J., and C. M. R. Platt, 1977: Lidar for multiple backscattering and depolarization observations. *Appl. Opt.*, **16**, 3193–3199.

Cox, S. K., 1976: Observations of cloud infrared effective emissivity. *J. Atmos. Sci.*, **33**, 287–289.

Davis, P. A., 1970: Applications of an airborne ruby lidar during a BOMEX period of cirrus observations. *J. Appl. Meteor.*, **10**, 1314–1323.

Griffith, K. T., and S. K. Cox, 1977: Infrared radiative properties of tropical cirrus clouds inferred from broadband measurements. Atmos. Sci. Pap. No. 269, Colorado State University, 102 pp.

Hall, F. F., Jr., 1968: A physical model of cirrus 8 μm to 13 μm radiance. *Appl. Opt.*, **7**, 2264–2269.

Heymsfield, A. J., and R. G. Knollenberg, 1972: Properties of cirrus generating cells. *J. Atmos. Sci.*, **29**, 1358–1366.

Hubert, L. F., 1975: Note on jet cirrus emissivity. *Quart. J. Roy. Meteor. Soc.*, **101**, 1017–1019.

Kuhn, R. M., and H. K. Weickmann, 1969: High altitude radiometric measurements of cirrus. *J. Appl. Meteor.*, **8**, 147–154.

Paltridge, G. W., and C. M. R. Platt, 1976: *Radiative Processes in Meteorology and Climatology*. Elsevier, 318 pp.

Platt, C. M. R., 1971: A narrow-beam radiometer for atmospheric radiation studies. *J. Appl. Meteor.*, **10**, 1307–1313.

——, 1973: Lidar and radiometric observations of cirrus clouds. *J. Atmos. Sci.*, **30**, 1191–1204.

——, 1975: Infrared emissivity of cirrus—simultaneous satellite, lidar and radiometric observations. *Quart. J. Roy. Meteor. Soc.*, **101**, 119–126.

——, 1979: Remote sounding of high clouds: I. Calculation of visible and infrared optical properties from lidar and radiometer measurements. *J. Appl. Meteor.*, **18**, 1130–1143.